Iranian Journal of Materials Forming 6 (1) (2019) 44-55

Online ISSN: 2383-0042

IJMF

Iranian Journal of Materials Forming

Journal Homepage: http://ijmf.shirazu.ac.ir

Flow Stress Modeling in a γ-γ′ Cobalt Base Superalloy by Using the Hyperbolic Sine Equation and ANN Method

S. Aliakbari Sani[1], H. Arabi[1], Sh. Kheirandish[1] and G.R. Ebrahimi[2*]

[1] School of metallurgy and Materials Engineering, Iran University of Science and Technology, Tehran, Iran
[2] Department of Materials Science and Engineering, Hakim Sabzevari University, Sabzevar, Iran

ARTICLE INFO

Article history:

Received 23 November 2018
Revised 28 January 2019
Accepted 18 February 2019

Keywords:

γ-γ′ Co-base superalloys
Hot deformation modeling
Flow stress prediction
Hyperbolic sine equation
ANN

ABSTRACT

The new class of wrought γ-γ′ Co-base superalloys, which are based on Co-Al-W system, was developed by conventional hot working routes with a high volume fraction of γ′ precipitates and good mechanical properties. The aim of the present study was to predict the flow stress and hot deformation modeling of a novel γ-γ′ Co-base superalloy. The hot compression tests were carried out over a wide range of temperatures (950°C-1200°C) and strain rates ($0.001s^{-1}$-$1s^{-1}$). The flow stress analysis, constitutive approach and microstructure characterization revealed that dynamic recrystallization (DRX) occurred at a high temperature regime (1100°C-1200°C) but not at a low one (950°C-1050°C) due to the presence of γ′ precipitates. The hot deformation characteristic was studied using the hyperbolic sine equation on each of the above-mentioned regimes and the ANN approach on the overall conditions. The constitutive method indicated good potential for the prediction of the flow stress at each separated regime, but the ANN model represented a much more appropriate performance. The outstanding predictability of the ANN model regardless of the γ′ phase participation during the thermomechanical processing under the overall deformation conditions can be considered as another achievement of the proposed approach.

1. Introduction

New Co-base superalloys, based on Co-Al-W system and strengthened by the ordered γ′ phase, $L1_2$ structure and Co_3 (Al, W) composition, were first introduced in 2006 [1] and then studied by many researchers [2-5]. It is reported [4-7] that in cast alloy of this type, high temperature mechanical properties are comparable to those of the well-known Ni-base superalloys such as IN713, MarM247, and CMSX-3. The high temperature stability, high volume fraction (up to 90%), and proper anti-phase boundary (APB) energy of γ′ precipitates were assumed to be the superior properties [4, 5, 8-10].

The wrought Ni-base superalloys containing the γ′ phase were usually used in gas turbines as disc, blade, hub and shaft parts. The wrought superalloys have been conventionally fabricated by ingot metallurgy, which involves several thermomechanical processes on cast material known as the cogging treatment. Waspaloy, Udimet720 and IN718 are generally prepared by this approach [11, 12]. However, in modern alloys such as RR1000 and Rene 95, which contain a high volume fraction of γ′ precipitates and superior mechanical properties, the cogging treatment cannot be applied due to the high γ′ solvus temperature. In other words, their hot working temperature range is interposed on the stability domain of γ′, and then on the hot deformation process along with crack and failure [11, 13]. Fortunately, it was shown [4, 5, 14, 15] that the temperature range between the γ′ solvus and solidus temperatures, as hot working window, of Co-Al-W alloys is larger than that of many wrought Ni-base

* Corresponding author
E-mail addresses: ebrahimi@hsu.ac.ir (GH. Ebrahimi)

superalloys. Besides, in the Co-Al-W superalloys, especially those alloyed with Ta, Ti and Ni elements, the volume fraction of the γ' phase of more than 70% can be obtained. Therefore, it can be considered as a high strength superalloy with appropriate workability as well as excellent high temperature properties [16, 17]. It reveals that the wrought specimens can be fabricated by the conventional thermomechanical treatments such as hot rolling [17-19] and hot pressing [20]. To the best knowledge of the author, no systematic research has been so far conducted to investigate hot deformation mechanisms, variables and parameters.

The hot deformation processes of alloys are usually accompanied with complex conditions and multifaceted variables such as initial microstructure, present phases and processing parameters (temperature, strain, strain rate, inter-pass time). Therefore, predicting the flow stress and hot deformation modelling has been of great importance in different industrial units. In the field of metal working, finite element method (FEM) is used as a useful tool to simulate the thermomechanical process and find out the optimum parameters. The constitutive equation which presents the material's flow behavior is used as input to the FEM code for simulating the material's response under specified loading conditions. Therefore, the reliability of these simulations' outputs depends essentially on the modeling of the constitutive equation [21]. The hot deformation models are divided into three main categories: 1- phenomenology models, 2- physical models and 3- Artificial Neural Network (ANN) approach [22, 23]. The phenomenology models are based on macro parameters, not taking micro mechanisms into account. The main phenomenology models are Johnson–Cook (JC) [24, 25], Khan-Huang-Liang (KHL) [26, 27], Molinari–Ravichandran (MR) [22] and various Arrhenius equations [28-30]. The physical models are based on the material's thermodynamic path, dislocation movement, activation energy and slip dynamics such as Zerilli–Armstrong [31], MTS [32], Preston–, and Voyiadjis–Almasri [33]. Modeling by using physical types has higher levels of accuracy compared to phenomenology ones; however, their equation forms are quite complex and the parameters obtained in these models are difficult. This is despite the fact that the parameters and constants of both models are based on data regression analysis through hot deformation parameters which often have a nonlinear relationship with the flow stress [22].

Artificial neural networks (ANN) are a category of parallel processing architectures, which can mimic complex relationships at various phenomena and subjects. The attraction of the ANN methods is that they are best suited to solve the problems that are the most difficult to solve by the statistical, numerical or traditional computational methods. In this approach, the relationship between the parameters can be learned by a network through adequate training based on initial and/or experimental data. Not only can it make decisions using incomplete and disorderly information, but it also can generalize rules through training and apply these rules to new cases. Usually the structure design of an ANN is divided into 3 layers: input, hidden and output. The ANN is a useful approach to solve complex problems in various materials science fields [34-38], especially in hot working [39-41].

The modeling and simulation approaches using hot compression tests are a common way of assessing the high temperature behavior of a material at various conditions. Therefore, due to the production of Co-Al-W superalloy as a wrought form by thermomechanical treatment, it is necessary to predict the flow stress and its relationship with hot working parameters. In addition, to describe the hot deformation behavior during the thermomechanical processing, it can be studied and predicted by establishing a model. The aim of the present research is the hot deformation modeling of a cast Co-Al-W superalloy by using the hyperbolic sine constative equation and ANN approach based on the hot compression tests.

2. Material and Methods

The designed superalloy was prepared by a vacuum induction melting (VIM) furnace, and then poured into a ceramic mold. The chemical composition of the as-cast alloy was obtained as 9.8Al-7.4W-2.7Ti-20.4Ni-0.4C-0.1B (at %) by an inductively coupled plasma atomic emission spectroscopy (ICP-OES), thermo iCAP 6000,

and LECO TS 230 carbon analyzer instruments. The differential scanning calorimetry (DSC) thermal analysis was used to measure the γ' solution/precipitation temperatures considering 10°C.min^{-1} in heating/cooling rate under nitrogen protective gas, as shown in Fig. 1. The critical solvus and precipitate temperatures were calculated at about 1079ºC and 1071ºC, respectively.

The as-cast sample was homogenized at 1300°C temperature through 16 hours, according to our previous work [42]. The cylindrical samples with a diameter of 8mm and height of 12mm, according to ASTM-E209, were machined out from the homogenized alloy using the wire-cut electro-discharge machine. A Zwick/Roell Z250 testing machine equipped with a computerized control furnace was used to perform the hot compression tests in a temperature range of 950°C-1200°C and strain rates of 0.001-1s^{-1}, up to true strain of 0.4. The samples were then held at the test temperature for 5 min., prior to hot compression, and quenched immediately after the test to maintain the hot worked microstructure. Optical microscopy and field emission gun scanning electron microscopy (FEGSEM) were employed to examine the deformation-induced microstructures. Having been ground and polished, the samples were etched in waterless Kalling and Glyceregia [43] solutions for deformed and sub-micron structures that were obtained by OM and FEGSEM equipment, respectively. In addition, a FE-SEM (Philips XL30S-FEG), equipped with electron back scatter diffraction (EBSD) detector, was utilized and the data obtained from EBSD were analyzed using TSL-OIM.

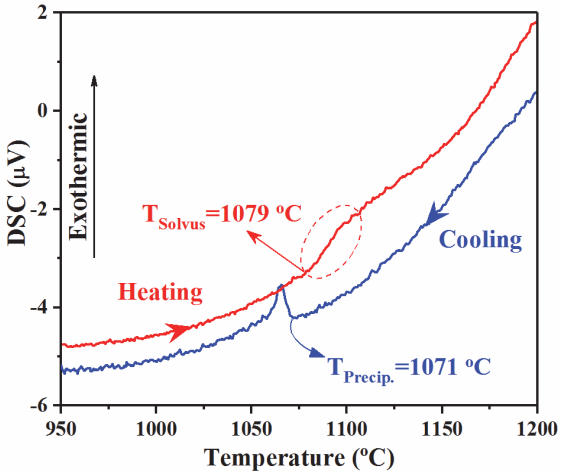

Fig. 1. The DSC result of the as-cast alloy during heating and cooling routs

3. Results and Discussion

3.1. Flow curves and microstructure

Different levels of the alloy's flow stress at various strain rates (0.001s^{-1}-1s^{-1}) are presented in Fig. 2 It can be seen that the true levels of the stress decline by increasing the temperature and decreasing the strain rate. Fig. 2 clearly indicates that the stress level at a low temperature regime (950°C, 1000°C, 1050°C) is higher than that of a high temperature regime (1100°C, 1150°C, 1200°C). By paying careful attention to the resultant γ' precipitation temperature (1071°C), the hot compression tests can be divided into two regimes, i.e. low and high ones.

The hyperbolic sine constitutive equation is an accepted methodology to describe the hot working behavior of many alloys at various temperatures and strain rates, which can be expressed as follows [29, 44, 45]:

$$Z = \dot{\varepsilon}\exp(\frac{Q}{RT}) = A[\sinh(\alpha\sigma)] \quad (1)$$

Here, Z is the Zener-Hollomon parameter; $\dot{\varepsilon}$ and T are the strain rate and temperature of the deformation test, respectively. Q denotes the activation energy and n is the stress power; besides, R, A and α are the constants. The value for the constants of the above equation at both regimes is calculated at the strain of 0.2, according to the approach which was explained briefly in the literature [46].

Table 1. The hot working parameters based on the hyperbolic sine equation with a strain rate of 0.2 at low and high temperature regimes

	α	n	Q	lnA
Low temperature regime	0.0026	9.15	1196	107.40
High temperature regime	0.0103	4.16	511.74	55.78

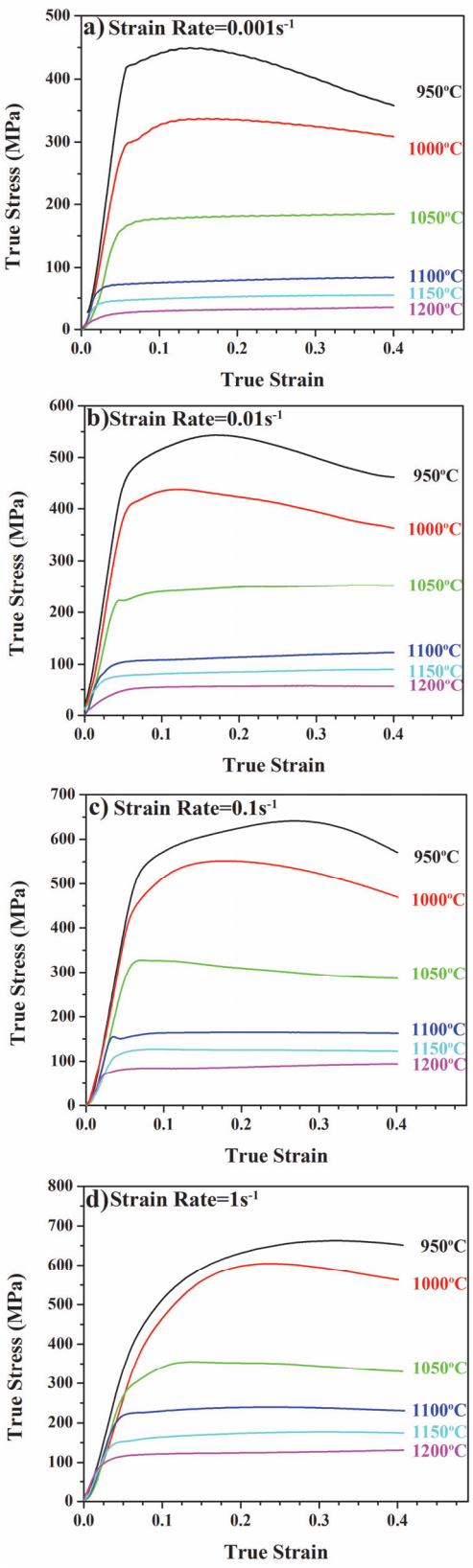

Fig. 2. The experimental flow curves of the studied alloy at different temperatures and strain rates of: a) $0.001s^{-1}$, b) $0.01s^{-1}$, c) $0.01s^{-1}$ and d) $1s^{-1}$

The resultant data are presented in Table 1. According to this table, there is an obvious difference between these parameters at both regimes, which is related to the distinct mechanism(s) during the hot deformation of each regime. The Q and n values at the high temperature regime are 1196.52kj.mol^{-1} and 4. 16, respectively; however, at the low temperature regime, these parameters are 511.74kj.mol^{-1} and 4.16, respectively. It is noteworthy that both resultant Qs are more than one for the self-diffusion of the Co element (286 kj.mol^{-1} [47]), especially in the low temperature regime. The Q value for the high temperature regime (511.74 kj.mol^{-1}) is similar to the Q values for some nickel-base superalloys [48-52], having no gamma prime phase during the hot working, i.e. within a range 400 to 491 kj.mol^{-1}, due to the happening of the dynamic recrystallization phenomena [49-51]. However, the high Q value at the low temperature regime (1182.48 kj.mol^{-1}) can be compared with that of Udimet 720 (1552 kj.mol^{-1} [53]) and Waspaloy (1400 kj.mol^{-1} [49]) which are deformed below the gamma prime phase precipitation temperature.

The deformed microstructures of the alloy at a strain rate of 0.01 s^{-1} and temperatures of 1000°C and 1150°C are shown in Fig. 3. In the micrograph taken at the low temperature regime (Fig. 3-a, b), it can be seen that the large initial as-cast grains impose some strain but this deformation causes flow instability. The FE-SEM micrographs (Fig. 3-c) show some slip bands which contain many sheared dislocation-pairs [10, 54, 55], assistion the cracks to occur along these bands, which finally lead to fracture, as can be seen in Fig. 3-a.

In contrast, some new grains were found at the high temperature regime (Fig. 3-d, e, f), which appeared by the Dynamic recrystallization (DRX) phenomenon. Both the flow curves and deformed microstructure can be related to the initial microstructure before performing the hot compression tests in every designed regime. More details about the mechanisms and activated phenomena were investigated by the authors elsewhere [56].

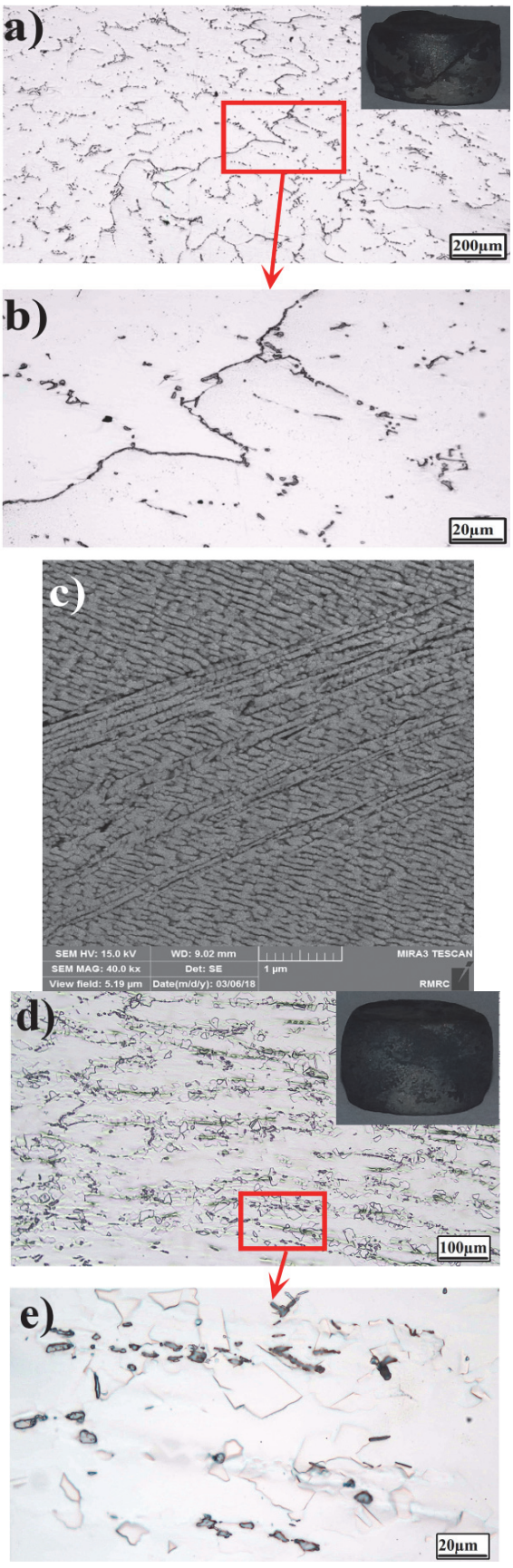

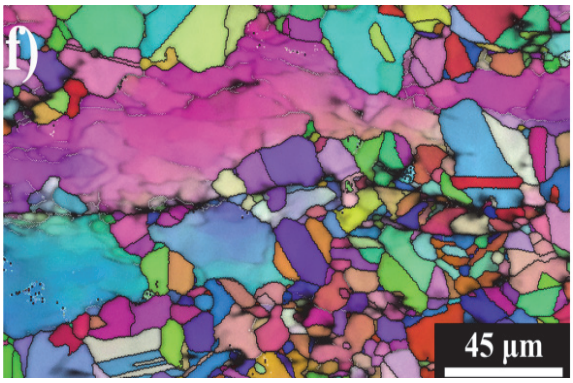

Fig. 3. The hot deformed microstructure at the strain rate of $0.01s^{-1}$ and temperatures of 1000°C (a, b, c) and 1150°C (d, e, f)

The starting microstructures of the studied alloy, exactly just before the deformation, at 950°C, 1000°C, 1050°C and 1150°C are shown in Fig. 4 The high volume fraction and small size of the γ' particles at the low temperature regime are shown in Fig a, b, c. however, the evidence of the gamma prime phase was not detected at any other conditions Fig. 4 (d). In other words, the studied alloy with a specified composition was partitioned into two distinct microstructures with different hot deformation behaviors.

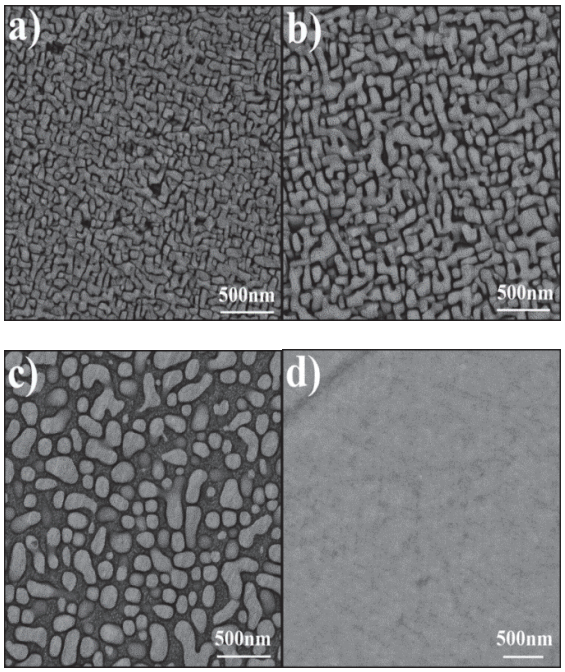

Fig. 4. The starting microstructures just before the deformation at temperatures of a (950°C, b) 1000°C, (c) 1050°C and (d) 1150°C

3.2. Hyperbolic sine modeling

Considering Eq. (1), the hyperbolic sine equation that relates the stress of the hot deformation to the Zener-Hollomon parameter can be expressed as:

$$\sigma = (\frac{1}{\alpha})[\sinh^{-1}(\frac{Z}{A})]^{(\frac{1}{n})} \quad (2)$$

To predict the variation of the flow stress of the hot deformation with strain, the material constants (i.e. α, n, Q and A) must be calculated at every specific strain. These values at various strains (0.1-0.4) are obtained with similar procedure described above and presented in Fig. 5.

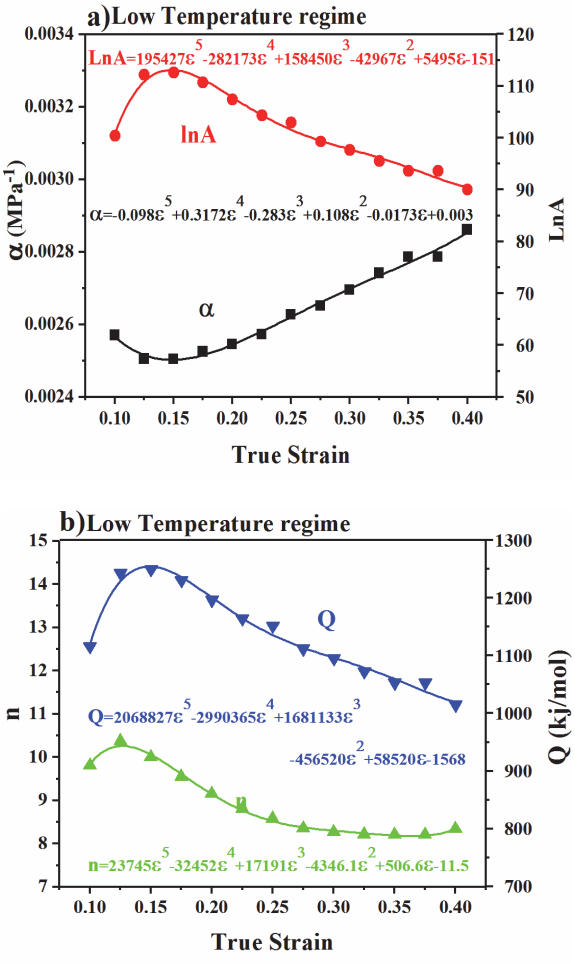

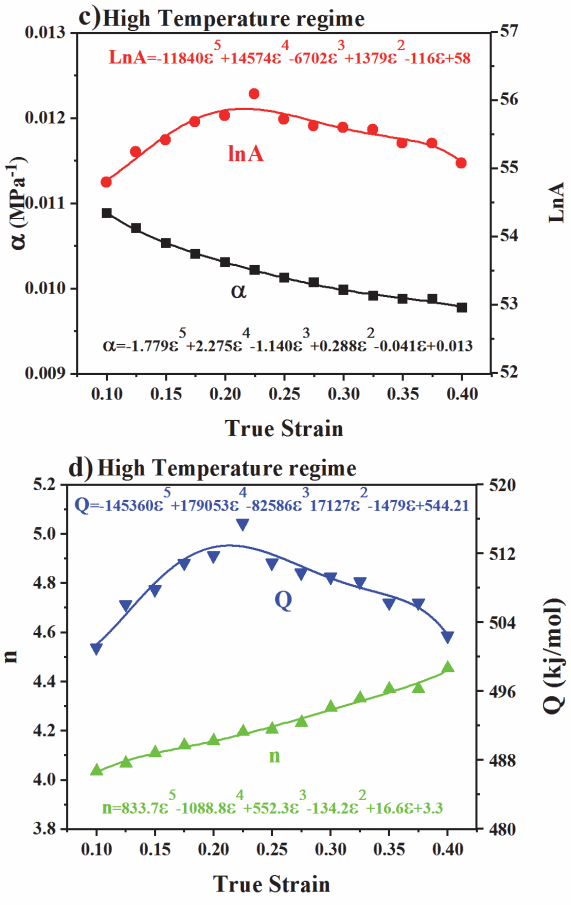

Fig. 5. The variation of the hot deformation constants (α, ln A, n, Q) of the hyperbolic sine equation as a function of true strain at low and high temperature regimes

It is accepted that the material constants' variation with the strain is using the polynomial function [51, 57]. In this regard, the 5th order polynomial function is used according to the typical form (3), as well as every function calculated and presented in Fig. 5.

$$f(\varepsilon) = a_5\varepsilon^5 + a_4\varepsilon^4 + a_3\varepsilon^3 + a_2\varepsilon^2 + a_1\varepsilon + a_0 \quad (3)$$

Finally, the predicted flow stress was calculated by Eq. (2). The predicted stress and the experimental data at the strain rates are shown in Fig. 6 It can be seen that the predicted stress level in the high temperature regime is not that different from the experimental data. However, at the low temperature regime, there is a gap in the predicted results. This may be related to the variation of the volume fractions and size of the gamma prime precipitates which are formed before the compression test and affect the hot deformation behavior.

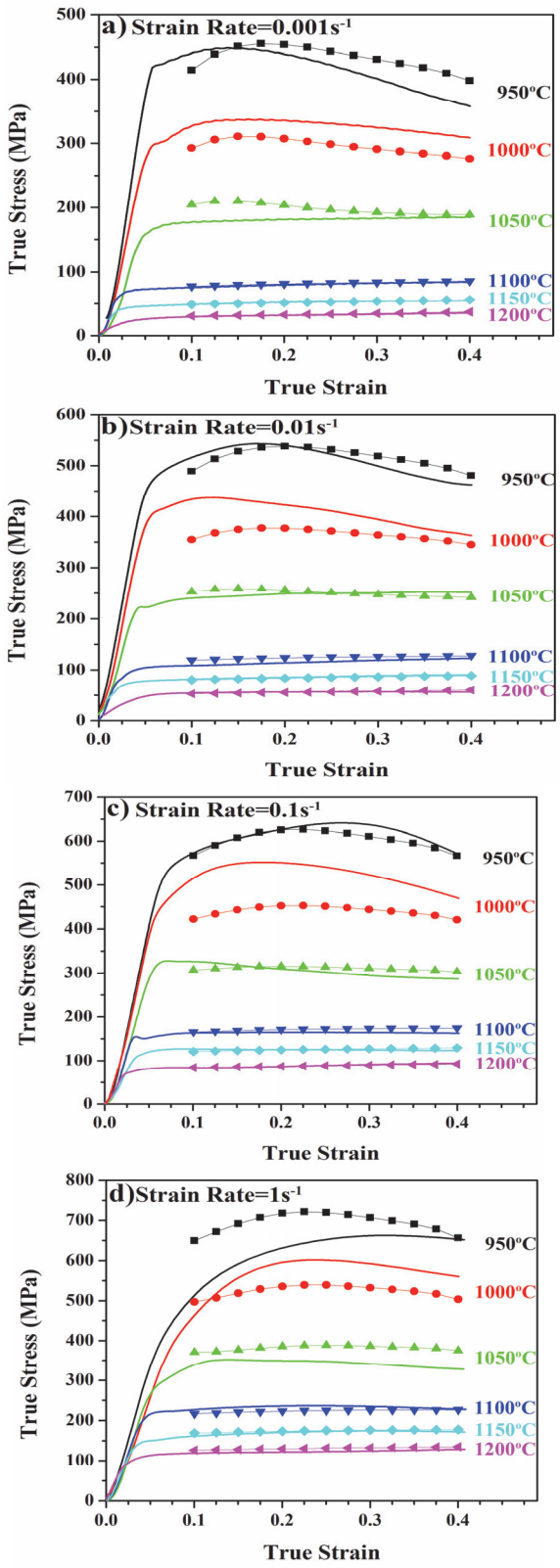

Fig. 6. The prediction of the stress from the hyperbolic sine equation modeling and experimental data at different temperatures and strain rates of: a) $0.001s^{-1}$, b) $0.01s^{-1}$, c) $0.01s^{-1}$ and d) $1s^{-1}$ (the solid line and pointed-line curves show the experimental data and prediction, respectively)

3.3. ANN modeling

In the current study, the back propagation artificial neural network (BP-ANN) was used for the flow stress prediction of the studied alloy at the overall conditions without any predefined temperature regimes. The temperature, the strain rate and the strain were introduced to the network as the input data and the stress was assumed to be the output data. The set of the input data, obtained from the hot compression tests, was validated by using the temperature (950°C to 1200°C), logarithm of the strain rate (-3 to 0) and strain (0.1 to 0.4). The set of the input, read by the network, was normalized by the following equation within the range of 0.1-0.9 [58]:

$$X' = 0.1 + 0.8\left(\frac{X - X_{Min}}{X_{Max} - X_{Min}}\right) \quad (4)$$

Where X is the original data, X_{max} and X_{min} values are the maximum and minimum data for X respectively, and X' is the normalized data. The number of the neurons in the hidden layer is determined by several trail-error methods, and the statistical adequacy model was evaluated with mean square error (MSE). The MSE of the network reached its minimum value when the number of the hidden layer neurons was 12. The schematic diagram of the network architect is presented in Fig. 7 In this approach, 132 data were randomly selected from 176 points (75% of the data) as the inputs for the training phase of the BP-ANN network.

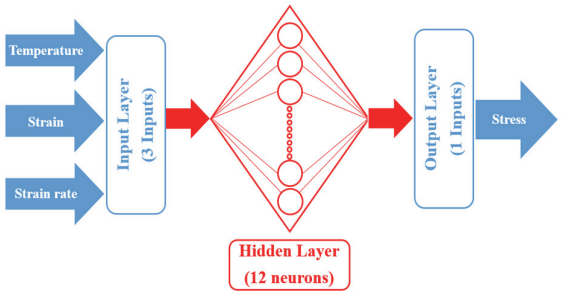

Fig. 7. The schematic diagram of the network used in this study.

The ANN predicted stress obtained after the training of the network as well as the experimental data are presented in Fig. 8 As seen clearly, the ANN predicted values can correctly and properly at various conditions.

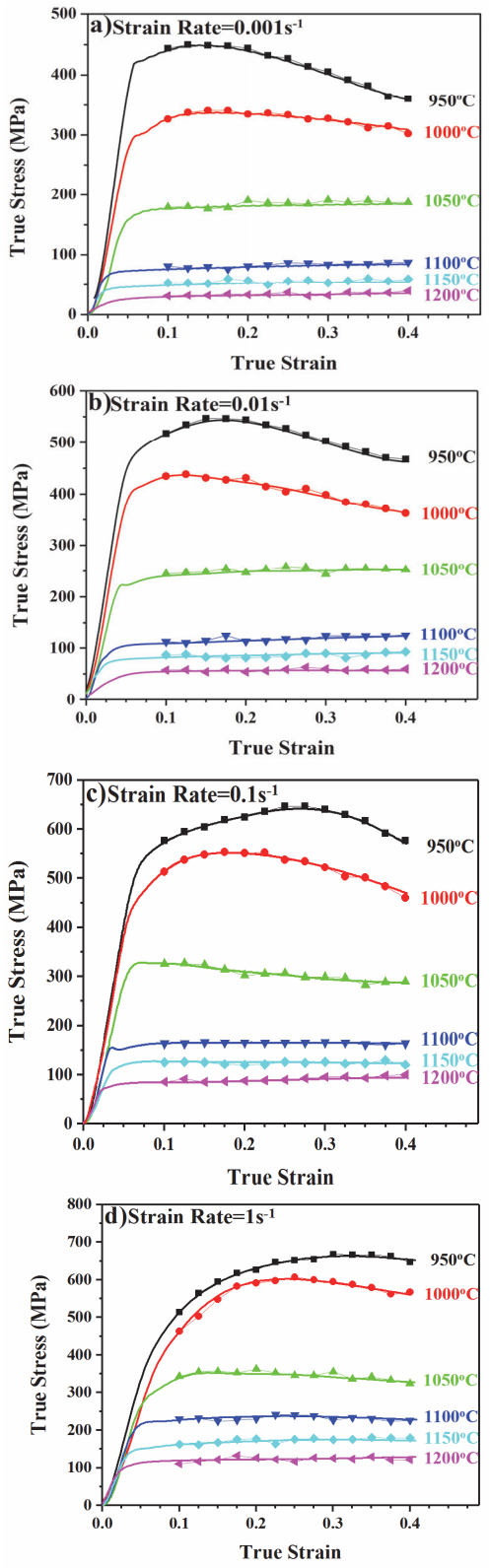

Fig. 8. The prediction stress from the ANN modeling and experimental data at different temperatures and strain rates of: a) 0.001s^{-1}, b) 0.01s^{-1}, c) 0.01s^{-1} and d) 1s^{-1} (solid line and pointed line curves show experimental and prediction, respectively)

Table 2. The correlation coefficient (R) and average absolute relative error (AARE) at the two used models

Method	R	AARE
Hyperboilic sine, Low temperature regime	0.954	4.493
Hyperboilic sine, High temperature regime	0.995	1.829
ANN, over all data	0.999	0.897

3.4. Verification and comparison of the models

The plot of the experimental flow stress data and predicted values by the hyperbolic sine equation at both regimes and the ANN approach at the overall data are shown in Fig. 9 The predictability of the two models is further quantified by employing the standard statistical parameters such as correlation coefficient (R) and average absolute relative error (AARE), which are expressed bellow, where $\sigma^i_{exp.}$ is the experimental flow stress, σ^i_p is the predicted flow stress, and $\sigma^m_{exp.}$ and $\sigma^m_{exp.}$ are the mean values of $\sigma^i_{exp.}$ and σ^i_p, respectively and N is the total number of data.

$$R = \frac{\sum_{i=1}^{N}(\sigma^i_{exp.}-\sigma^m_{exp.})(\sigma^i_p-\sigma^m_p)}{\sqrt{\sum_{i=1}^{N}(\sigma^i_{exp.}-\sigma^m_{exp.})^2(\sigma^i_p-\sigma^m_p)^2}} \quad (5)$$

$$AARE = \frac{1}{N}\sum_{i=1}^{N}\left|\frac{\sigma^i_{exp.}-\sigma^i_p}{\sigma^i_{exp.}}\right| \quad (6)$$

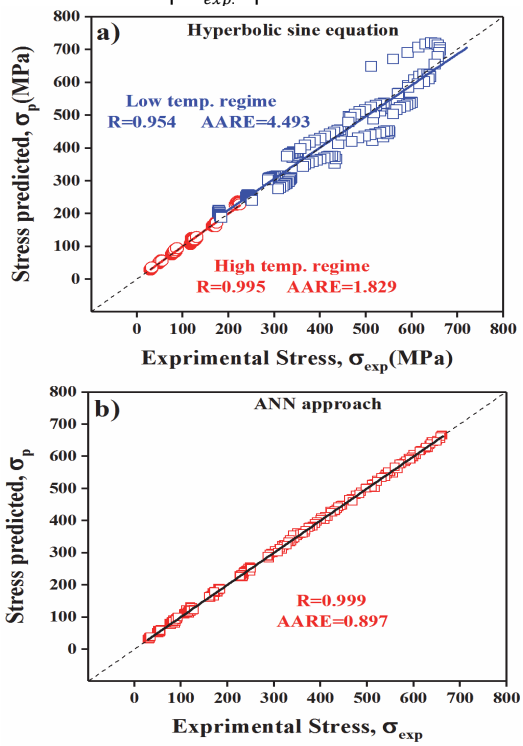

Fig. 9. Correlation between the experimental and predicted flow stress by using a) hyperbolic sine equation and b) ANN approach

These parameters were calculated for both models and are presented in Table 2. According to the prediction results Fig. 9 as well as the statistical parameters (Table 2), it can be said that a good correlation is obtained by the constative equation model, especially at the high temperature regimes. However, the ANN model presented relatively much more accurate results at the extended hot deformation domain. The neural network with the mentioned optimum architecture was successfully incorporated to numerically model the hot deformation characteristics of the investigated alloy. Moreover, as indicated in the results, the well-trained ANN has better prediction capability over the strain compensated constitutive model, regardless of the presence or absence of the γ' phase throughout the hot working. The suggested methodology proposed in the current work confirms the excellent capability of the ANN model in simulating complex multi-factors during the hot deformation of this cobalt based superalloy.

4. Conclusions

In this research, the high temperature flow behavior of a new cobalt based superalloy containing the γ' phase, with precipitation temperature of 1071ºC, was studied over the temperature domain of (950ºC-1200ºC) and strain rate range of ($0.001s^{-1}$-$1s^{-1}$). The results show that at the low temperature regime (950ºC-1050ºC) which contain the γ' phase, the hot deformation was accompanied with sole work hardening without DRX. Furthermore, at the high temperature regime (1100ºC-1200ºC), with a complete solution of the γ' phase, DRX occurred and proved to be the dominant restoration mechanism during the hot working. According to the hyperbolic sine equation, two distinct behaviors were seen at both regimes as Q values at the low and high temperature regimes were calculated at 1196.52 kj/mol.K and 511.74 kj/mol. K, respectively. The hyperbolic sine equation notwithstanding, the ANN approach was used to model the true stress-strain curves of the alloy at high temperatures not considering the presence or absence of the γ' phase throughout the deformation. The results indicate that although the constitutive equation could work well to predict the flow stress at every individual regime, the ANN yields more precise findings at the overall domain regardless of the partitioning of the working temperature range.

5. References

[1] J. Sato, T. Omori, K. Oikawa, I. Ohnuma, R. Kainuma and K. Ishida, Cobalt-Base High-Temperature Alloys, *Science*, 312 (2006) 90-91.

[2] T. Omori, K. Oikawa, J. Sato, I. Ohnuma, U. R. Kattner, R. Kainuma and K. J. I. Ishida, Partition behavior of alloying elements and phase transformation temperatures in Co–Al–W-base quaternary systems, 32 (2013) 274-283.

[3] S. Kobayashi, Y. Tsukamoto, T. Takasugi, H. Chinen, T. Omori, K. Ishida and S. J. I. Zaefferer, Determination of phase equilibria in the Co-rich Co–Al–W ternary system with a diffusion-couple technique, 17 (2009) 1085-1089.

[4] A. Bauer, S. Neumeier, F. Pyczak, R. Singer and M. Göken, Creep properties of different γ′-strengthened Co-base superalloys, *Materials Science and Engineering: A*, 550 (2012) 333-341.

[5] A. Suzuki and T. M. Pollock, High-temperature strength and deformation of γ/γ′ two-phase Co–Al–W-base alloys, *Acta Materialia*, 56 (2008) 1288-1297.

[6] F. Xue, H. Zhou, X. Chen, Q. Shi, H. Chang, M. Wang, X. Ding and Q. Feng, Creep behavior of a novel Co-Al-W-base single crystal alloy containing Ta and Ti at 982 °C, *MATEC Web of Conferences*, 14 (2014), 15002.

[7] M. S. Titus, A. Suzuki and T. M. Pollock, Creep and directional coarsening in single crystals of new γ–γ′ cobalt-base alloys, *Scripta Materialia*, 66 (2012) 574-577.

[8] K. Tanaka, M. Ooshima, N. Tsuno, A. Sato and H. Inui, Creep deformation of single crystals of new Co–Al–W-based alloys with fcc/L12 two-phase microstructures, *Philosophical Magazine*, 92 (2012) 4011-4027.

[9] A. Suzuki, H. Inui and T. M. J. A. R. o. M. R. Pollock, L12-strengthened cobalt-base superalloys, 45 (2015) 345-368.

[10] N. L. Okamoto, T. Oohashi, H. Adachi, K. Kishida, H. Inui and P. J. P. M. Veyssière, Plastic deformation of polycrystals of Co3 (Al, W) with the L12 structure, 91 (2011) 3667-3684.

[11] R. C. Reed, The superalloys: fundamentals and applications, Cambridge university press, 2008.

[12] M. J. Donachie and S. J. Donachie, Superalloys: a technical guide, ASM international, 2002.

[13] C. Cui, D. Ping, Y. Gu and H. Harada, A new Co-base superalloy strengthened by γ′ phase, *Materials transactions*, 47 (2006) 2099-2102.

[14] A. Bauer, S. Neumeier, F. Pyczak and M. Göken, Microstructure and creep strength of different γ/γ′-strengthened Co-base superalloy variants, *Scripta Materialia*, 63 (2010) 1197-1200.

[15] K. Shinagawa, T. Omori, J. Sato, K. Oikawa, I. Ohnuma, R. Kainuma and K. Ishida, Phase Equilibria and Microstructure on γ′ Phase in Co-Ni-Al-W System, *Materials Transactions*, 49 (2008) 1474-1479.

[16] S. Neumeier, L. P. Freund and M. Göken, Novel wrought γ/γ′ cobalt base superalloys with high strength and improved oxidation resistance, *Scripta Materialia*, 109 (2015) 104-107.

[17] K. Shinagawa, T. Omori, K. Oikawa, R. Kainuma and K. Ishida, Ductility enhancement by boron addition in Co–Al–W high-temperature alloys, *Scripta Materialia*, 61 (2009) 612-615.

[18] H.-Y. Yan, V. A. Vorontsov, J. Coakley, N. G. Jones, H. J. Stone and D. J. S. Dye, Quaternary alloying effects and the prospects for a new generation of Co-base superalloys, 53 (2012) 705.

[19] H.-Y. Yan, J. Coakley, V. A. Vorontsov, N. G. Jones, H. J. Stone and D. Dye, Alloying and the micromechanics of Co–Al–W–X quaternary alloys, *Materials Science and Engineering: A*, 613 (2014) 201-208.

[20] E. T. McDevitt, Vacuum induction melting and vacuum arc remelting of Co-Al-WX gamma-prime superalloys, *MATEC Web of Conferences*, 14 (2014), 02001.

[21] X. He, Z. Yu, G. Liu, W. Wang, X. J. M. Lai and Design, Mathematical modeling for high temperature flow behavior of as-cast Ti–45Al–8.5 Nb–(W, B, Y) alloy, 30 (2009) 166-169.

[22] Y. Lin and X.-M. Chen, A critical review of experimental results and constitutive descriptions for metals and alloys in hot working, *Materials and Design*, 32 (2011) 1733-1759.

[23] J. Wang, G. Zhao, L. Chen, J. J. M. Li and Design, A comparative study of several constitutive models for powder metallurgy tungsten at elevated temperature, 90 (2016) 91-100.

[24] G. R. Johnson and W. H. J. E. f. m. Cook, Fracture characteristics of three metals subjected to various strains, strain rates, temperatures and pressures, 21 (1985) 31-48.

[25] L. Chen, G. Zhao, J. J. M. Yu and Design, Hot deformation behavior and constitutive modeling of homogenized 6026 aluminum alloy, 74 (2015) 25-35.

[26] R. Liang and A. S. J. I. J. o. P. Khan, A critical review of experimental results and constitutive models for BCC and FCC metals over a wide range of strain rates and temperatures, 15 (1999) 963-980.

[27] A. S. Khan, Y. S. Suh and R. J. I. J. o. P. Kazmi, Quasi-static and dynamic loading responses and constitutive modeling of titanium alloys, 20 (2004) 2233-2248.

[28] J. Jonas, C. Sellars and W. M. J. M. R. Tegart, Strength and structure under hot-working conditions, 14 (1969) 1-24.

[29] C. M. Sellars and W. J. A. M. McTegart, On the mechanism of hot deformation, 14 (1966) 1136-1138.

[30] H. Mirzadeh, J. M. Cabrera and A. Najafizadeh, Constitutive relationships for hot deformation of austenite, *Acta materialia*, 59 (2011) 6441-6448.

[31] T. Billot, P. Villechaise, M. Jouiad and J. Mendez, Creep–fatigue behavior at high temperature of a UDIMET 720 nickel-base superalloy, *International Journal of fatigue*, 32 (2010) 824-829.

[32] W. Betteridge, The properties of metallic cobalt, *Progress in Materials Science*, 24 (1980) 51-142.

[33] D. L. Preston, D. L. Tonks and D. C. J. J. o. A. P. Wallace, Model of plastic deformation for extreme loading conditions, 93 (2003) 211-220.

[34] H. Bhadeshia, Neural networks in materials science, *ISIJ international*, 39 (1999) 966-979.

[35] M. Dashtbayazi, Artificial neural network-based multiobjective optimization of mechanical alloying process for synthesizing of metal matrix nanocomposite powder, *Materials and Manufacturing Processes*, 27 (2012) 33-42.

[36] S. Malinov, W. Sha and J. McKeown, Modelling the correlation between processing parameters and properties in titanium alloys using artificial neural network, *Computational materials science*, 21 (2001) 375-394.

[37] J. Ciurana, G. Arias and T. Ozel, Neural network modeling and particle swarm optimization (PSO) of process parameters in pulsed laser micromachining of hardened AISI H13 steel, *Materials and Manufacturing Processes*, 24 (2009) 358-368.

[38] M. Kundu, S. Ganguly, S. Datta and P. Chattopadhyay, Simulating time temperature transformation diagram of steel using artificial neural network, *Materials and Manufacturing Processes*, 24 (2009) 169-173.

[39] A. He, G. Xie, X. Yang, X. Wang and H. Zhang, A physically-based constitutive model for a nitrogen alloyed ultralow carbon stainless steel, *Computational Materials Science*, 98 (2015) 64-69.

[40] S. Mandal, P. Sivaprasad, P. Barat and B. Raj, An overview of neural network based modeling in alloy design and thermomechanical processing of austenitic stainless steels, *Materials and Manufacturing Processes*, 24 (2009) 219-224.

[41] Y. Qin, Q. Pan, Y. He, W. Li, X. Liu and X. Fan, Artificial neural network modeling to evaluate and predict the deformation behavior of ZK60 magnesium alloy during hot compression, *Materials and Manufacturing Processes*, 25 (2010) 539-545.

[42] S. Aliakbari Sani, H. Arabi, S. Kheirandish. and G. R. Ebrahimi, An Investigation on the Homogenization Treatment and Elements Segregation on the Microstructure of a γ/γ/ Cobalt Based Superalloy, *International Journal of Minerals, Metallurgy and Materials*, Accepted.

[43] M. Durand-Charre, The microstructure of superalloys, Routledge, 2017.

[44] H. McQueen and N. Ryan, Constitutive analysis in hot working, *Materials Science and Engineering: A*, 322 (2002) 43-63.

[45] A. Rollett, F. Humphreys, G. S. Rohrer and M. Hatherly, Recrystallization and related annealing phenomena, Elsevier, 2004.

[46] L. Liu and H. Ding, Study of the plastic flow behaviors of AZ91 magnesium alloy during thermomechanical processes, *Journal of Alloys and Compounds*, 484 (2009) 949-956.

[47] C. E. Campbell, W. J. Boettinger and U. R. Kattner, Development of a diffusion mobility database for Ni-base superalloys, *Acta Materialia*, 50 (2002) 775-792.

[48] M. Jahangiri, H. Arabi and S. Boutorabi, High-temperature compression behavior of cast and homogenized IN939 superalloy, *Metallurgical and Materials Transactions A*, 44 (2013) 1827-1841.

[49] A. Chamanfar, M. Jahazi, J. Gholipour, P. Wanjara and S. Yue, Evolution of flow stress and microstructure during isothermal compression of Waspaloy, *Materials Science and Engineering: A*, 615 (2014) 497-510.

[50] A. Momeni, S. Abbasi, M. Morakabati, H. Badri and X. Wang, Dynamic recrystallization behavior and constitutive analysis of Incoloy 901 under hot working condition, *Materials Science and Engineering: A*, 615 (2014) 51-60.

[51] S. A. Sani, A. Khorram, A. Jaffari and G. J. R. M. Ebrahimi, Development of processing map for InX-750 superalloy using hyperbolic sinus equation and ANN model, 1-10.

[52] C. Sun, J. Liu, R. Li, Q. Zhang and J. J. R. M. Dong, Constitutive relationship of IN690 superalloy by using uniaxial compression tests, 30 (2011) 81-86.

[53] H. Monajati, A. Taheri, M. Jahazi and S. Yue, Deformation characteristics of isothermally forged UDIMET 720 nickel-base superalloy, *Metallurgical and Materials Transactions A*, 36 (2005) 895-905.

[54] F. Zhong, Y. Yu, S. Li, J. J. M. S. Sha and E. A, In-situ SEM and TEM tensile observations of novel Co-Al-W-Mo-Ta-B-Ce alloys with a coherent γ-CoSS/γ'-Co3 (Al, W) microstructure at room temperature, 696 (2017) 96-103.

[55] X. Lv, F. Sun, J. Tong, Q. Feng, J. J. J. o. M. E. Zhang and Performance, Paired dislocations and their interactions with γ′ particles in polycrystalline superalloy GH4037, 24 (2015) 143-148.

[56] S. A. Sani, H. Arabi and G. R. Ebrahimi, Hot deformation behavior and DRX mechanism in a γ-γ/ Cobalt base superalloy, *Materials Science and Engineering: A*, submitted.

[57] Y. Ning, Z. Yao, X. Liang and Y. Liu, Flow behavior and constitutive model for Ni–20.0 Cr–2.5 Ti–1.5 Nb–1.0 Al superalloy compressed below γ′-transus temperature, *Materials Science and Engineering: A*, 551 (2012) 7-12.

[58] Y. Sun, W. Zeng, X. Ma, B. Xu, X. Liang and J. Zhang, A hybrid approach for processing parameters optimization of Ti-22Al-25Nb alloy during hot deformation using artificial neural network and genetic algorithm, *Intermetallics*, 19 (2011) 1014-1019.

مدلسازی تنش سیلان در یک γ-γ′ / کبالت پایه فوق‌العاده با استفاده از معادله سینوسی هیپربولیک و روش ANN

ساعد علی‌اکبری ثانی[۱]، حسین عربی[۱]، شهرام خیراندیش[۱] و غلامرضا ابراهیمی[۲]

۱- دانشکده مهندسی مواد و متالورژی، دانشگاه علم و صنعت ایران، تهران، ایران.
۲- دانشکده مهندسی مواد و پلیمر، دانشگاه حکیم سبزواری، سبزوار، ایران.

چکیـــده

سوپرآلیاژهای کارشده از نوع پایه کبالت حاوی فاز γ′ که بر مبنای سیستم Co-Al-W توسعه یافته‌اند، دارای کسر حجمی بالایی از رسوبات فاز گاماپرایم با خواص مکانیکی مناسب هستند که با روش‌های متداول شکل‌دهی گرم قابلیت تولید دارند. هدف از تحقیق حاضر پیش‌بینی تنش سیلان و مدل‌سازی رفتار کارگرم یک سوپرآلیاژ جدید پایه کبالت γ-γ′ است. آزمایش‌های فشار گرم در یک بازه دما وسیع (۹۵۰°C-۱۲۰۰°C) و نرخ کرنش گسترده (s^{-1}-۱s^{-1} ۰/۰۰۱) انجام شد. تحلیل منحنی‌های سیلان، مطالعه روابط ساختاری و بررسی ریزساختار نشان داد که در رژیم دمای بالای شکل‌دهی (۱۱۰۰°C-۱۲۰۰°C) پدیده تبلور مجدد دینامیکی (DRX) رخ داده است، در صورتی‌که در رژیم دمای پایین (۹۵۰°C-۱۰۵۰°C)، به علت حضور رسوبات گاماپرایم، پدیده DRX رخ نداده است. بررسی رفتار کارگرم با استفاده از رابطه سینوس هایپربولیک در هر دو رژیم دمایی و با استفاده از روش شبکه عصبی مصنوعی (ANN) در تمام دماها انجام شد. مدل‌سازی با روش روابط بنیادی نشان داد که پیش‌بینی تنش سیلان در هر دما به خوبی انجام شد، در حالی‌که با استفاده از روش ANN دقت بالاتری به‌دست آمد. همچنین روش ANN توانایی مدل‌سازی رفتار کارگرم، بدون اثرپذیری از حضور یا عدم حضور رسوبات فاز گاماپرایم را نشان داد.

واژه‌های کلیدی: سوپرآلیاژهای پایه کبالت γ-γ′، مدل‌سازی کارگرم، پیش‌بینی تنش سیلان، رابطه سینوس هایپربولیک، روش ANN